EuroIntervention 2018;13:e1794-e1803 published online jaa November 2017 ■ published online e-edition February 2018

Bench testing and coronary artery bifurcations: a consensus document from the European Bifurcation Club

John A. Ormiston[1,2,3]*, MBChB; Ghassan Kassab[4], PhD; Gerard Finet[5], MD; Yiannis S. Chatzizisis[6], MD; Nicholas Foin[7], PhD; Timothy J. Mickley[8], BSME; Claudio Chiastra[9], PhD; Yoshinobu Murasato[10], MD; Yutaka Hikichi[11], MD; Jolanda J. Wentzel[12], PhD; Olivier Darremont[13], MD; Kiyotaka Iwasaki[14], PhD; Thierry Lefèvre[15], MD; Yves Louvard[15], MD; Susann Beier[2], PhD; Hikmat Hojeibane[16], MS; Ashley Netravali[17], MS; Jeffery Wooton[18], PhD; Brett Cowan[2], MBChB; Mark W. Webster[3], MBChB; Pau Medrano-Gracia[16,19], PhD; Goran Stankovic[20], MD

1. Mercy Angiography, Auckland, New Zealand; 2. University of Auckland, Auckland, New Zealand; 3. Auckland City Hospital, Auckland, New Zealand; 4. California Medical Innovations Institute, San Diego, CA, USA; 5. Hôpital Cardiologique, Claude Bernard University, Lyon, France; 6. University of Nebraska Medical Center, Omaha, NE, USA; 7. National Heart Research Institute, Singapore; 8. Boston Scientific, Minneapolis, MN, USA; 9. Politecnico di Milano, Milan, Italy; 10. Kyushu Medical Center, Fukuoka, Japan; 11. Saga University School of Medicine, Saga, Japan; 12. Erasmus MC, Biomedical Engineering, Rotterdam, the Netherlands; 13. Clinique Saint Augustin, Bordeaux, France; 14. Waseda University, Tokyo, Japan; 15. Hôpital Privé Jacques Cartier, Massy, France; 16. Stentys, Paris, France; 17. Abbott Vascular, Santa Clara, CA, USA; 18. Medtronic Corp, Santa Rosa, CA, USA; 19. Uniservices, Auckland, New Zealand; 20. University of Belgrade, Belgrade, Serbia

This paper also includes supplementary data published online at: http://www.pcronline.com/eurointervention/130th_issue/292

KEYWORDS

- bifurcation
- in-stent restenosis
- left main
- miscellaneous

Abstract

This is a consensus document from the European Bifurcation Club concerning bench testing in coronary artery bifurcations. It is intended to provide guidelines for bench assessment of stents and other strategies in coronary bifurcation treatment where the United States Food and Drug Administration (FDA) or International Organization for Standardization (ISO) guidelines are limited or absent. These recommendations provide guidelines rather than a step-by-step manual. We provide data on the anatomy of bifurcations and elastic response of coronary arteries to aid model construction. We discuss testing apparatus, bench testing end-points and bifurcation nomenclature.

*Corresponding author: Mercy Angiography, PO Box 9911, Newmarket, Auckland, 1023, New Zealand.
E-mail: johno@mercyangiography.co.nz

SUBMITTED ON 01/04/2017 - REVISION RECEIVED ON 1st 30/08/2017 / 2nd 02/10/2017 / 3rd 02/11/2017 - ACCEPTED ON 10/11/2017

DOI: 10.4244/EIJ-D-17-00270

Abbreviations

ASTM	American Society for Testing Materials
CT	computed tomography
HK	Huo-Kassab
ISO	International Organization for Standardization
microCT	micro computed tomography
QCA	quantitative coronary angiography
3D	three-dimensional
US FDA	United States Food and Drug Administration

Introduction and objectives

A significant proportion of atherosclerotic plaques develop in coronary artery bifurcations, and percutaneous intervention in these regions carries higher risk of adverse events than elsewhere. *In vitro* bench testing can add to the anatomical and functional assessment of bifurcation lesions, guiding percutaneous therapeutic strategies. The US Food and Drug Administration (FDA) stipulates, in its extensive guidance for industry, that non-clinical (bench) testing should support the safety and effectiveness of intracoronary stents and their delivery systems (dsmica@fda.hhs.gov). The International Organization for Standardization (ISO) publication, ISO 25539-2, details minimum requirements for endovascular devices and methods of test that will enable their evaluation. Test parameters for consideration include evaluating the device at extreme dimensions, in clinically relevant conditions and assessing performance at the outer limits of physiologic variables such as blood pressure, vascular compliance, and anatomic variations. Testing in a water bath or relevant fluid bath at 37±2°C is recommended by the ASTM F2079-09 for evaluating bioresorbable scaffolds. These organisations provide detailed guidance for general testing of stents (for instance for corrosion, stress/strain, fatigue analysis, particulate evaluation and more) but provide minimal guidance for bench testing of stents in coronary bifurcations.

This document, developed under the auspices of the European Bifurcation Club, is intended to assist bench assessment of stents and other strategies in coronary bifurcations where US FDA or ISO guidelines are limited or absent. It represents a starting foundation, and is expected to evolve over time. The recommendations, generated by clinicians, scientists and engineers, provide general principles, rather than a step-by-step manual. In this consensus, we propose consistent nomenclature and methodologies to standardise testing of bifurcation interventional procedures.

Editorial, see page 1741

APPLICATIONS OF BENCH TESTING OF DEVICES IN CORONARY ARTERY BIFURCATIONS

In general, bench testing may evaluate different stents or scaffolds, different bifurcation treatment strategies, the local haemodynamic forces in bifurcations, validate quantitative coronary angiography (QCA) systems, and aid teaching of interventional techniques.

In the evaluation of QCA systems, precision-manufactured rigid Plexiglass models with bifurcation lesions have been contrast filled and imaged radiographically in different obliquities. The angiographic analysis can be compared with known diameters, lengths and angles of the model for assessing accuracy, precision, and reproducibility[1].

Given the strong connection between biological responses such as restenosis and thrombosis, and perturbations in wall shear stress, it is useful to compute shear stress. Since computational models are based on assumptions, it is important to measure the velocity field and hence the associated shear stress in the region of the bifurcation to validate the computational predictions. Particle image velocimetry is one powerful method that allows visualisation of flow velocities in complex flow fields, with excellent temporal and spatial resolution[2]. Other methods to validate numerical simulations include measurement of flow in up-scaled bifurcation models using magnetic resonance imaging[3].

Ideally, testing should be performed by an independent party to avoid selective testing, data interpretation or reporting[4].

ANATOMY OF BIFURCATION MODELS

The geometry and material characteristics of models used should be reported. Early in the history of bench testing, very useful information was derived by testing in models that had limited anatomical accuracy and lacked the elastic response of human coronary arteries[5]. However, future bifurcation models are likely to be more anatomically correct, obeying geometric scaling laws and be constructed from materials that have an appropriate elastic response to improve the clinical relevance of testing.

SCALING LAWS OF FLOW

There are geometric rules known as scaling laws associated with the geometry of a coronary bifurcation. Nearly a century ago, Murray formulated the flow-diameter relation between proximal vessel and the branches[6]. Based on this scaling law and the conservation of mass through a bifurcation, a cube relation was found between the diameter of the proximal vessel and the sum of the diameters of branches **(Figure 1)**. Although the power law relation holds, Murray's exponent of 3 has been disputed for coronary arteries with the Huo-Kassab (HK) model[7], showing a 7/3 exponent to be more precise **(Figure 1)**. The Finet model[8] is simpler and based on fractal arguments. It holds for Y-type but not T-type bifurcations **(Figure 1)**, and also does not hold where there is a large discrepancy between branch diameters[9]. The Murray and HK models provide the flow distribution through the bifurcation in addition to the diameter constraints **(Figure 1)**.

DIAMETERS OF CORONARY ARTERIES AT DIFFERENT BIFURCATIONS, USING DIFFERENT MEASUREMENT MODALITIES IN DIFFERENT PATIENT SUBSETS

The vessels in bifurcations have different diameters in different individuals, at different sites and in different patient subsets **(Table 1)**. The mean diameter of the left main coronary artery from different studies ranged from 3.5 mm[10] to 4.75 mm[11] **(Table 1)**. Some of this variation is likely to be due to the differences in imaging

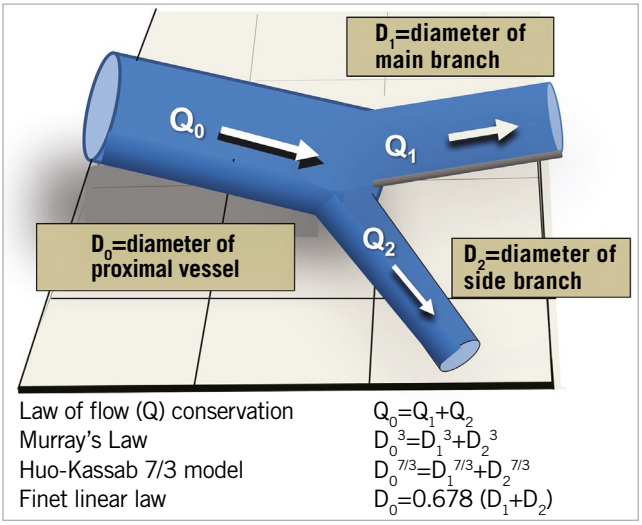

Figure 1. *Conservation of mass and the geometric relationship between vessel diameters in a bifurcation. In accordance with the law of conservation of mass, the sum of the flows in the two branches equals the flow in the proximal vessel[6-8]. The relationship of the diameters of the bifurcation vessels from three different authors is shown.*

technique with IVUS having higher resolution than invasive coronary angiography or CT angiography. Coronary artery diameters in bifurcations are larger in males than females[10]. There are likely to be differences in diameter between ethnic groups and at different ages[10]. The diameters of coronary arteries at different bifurcation sites, derived from an atlas of 300 patients without coronary artery disease, obtained from CT angiography, are shown in **Table 2**.

Coronary arteries taper. In a CT atlas, the tapering was 0.25 mm per 10 mm arterial length[10] and in an intravascular ultrasound study it was 0.22 mm per 10 mm of artery[12]. The tapering was less in the right coronary artery than in the left anterior descending or circumflex coronary arteries[12]. Tapering is not gradually progressive, but occurs abruptly after each vessel branch.

NOMENCLATURE FOR ANGLES BETWEEN CORONARY BIFURCATION BRANCHES

In a bifurcation, the angle between the proximal vessel and the side branch is called angle A **(Figure 2)**, that between the main branch and the side branch is angle B, and that between the proximal vessel and the main branch is angle C[13-16]. Since bifurcations are 3D structures, there is also an inflow angle between the proximal vessel and the plane of the branches **(Figure 2)**[10,16].

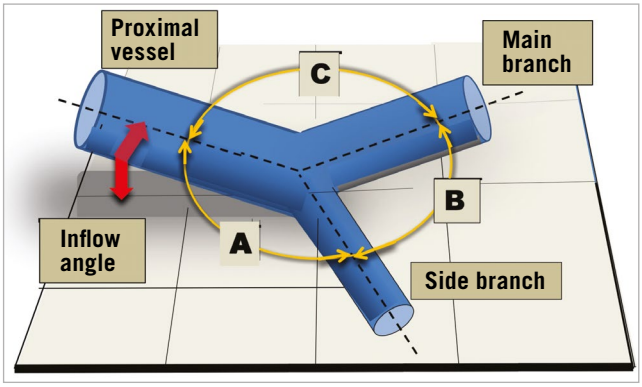

Figure 2. *Nomenclature for the angles between bifurcation branches. Angle A is that between the proximal vessel and the side branch. Angle B is between the main branch and the side branch. Angle C is between the proximal vessel and the main branch. The inflow angle is between the proximal vessel and the plane of the branches.*

Table 1. Diameters of the left main coronary artery and its branches assessed by different modalities.

	Number	Normal/ diseased	Modality	Sex	Left main bifurcation			Dm/ (D_1+D_2) (Finet ratio)
					L main (mm)	LAD (mm)	LCx (mm)	
Motreff[36]	52	Normal	IVUS	Both	4.20±0.8	3.37±0.5	3.28±0.7	0.63
Abizaid[11]	122	CAD	IVUS	Both	4.75*			
Finet[34]	41	Normal	QCA	Both	4.40±0.56	3.54±0.14	3.02±0.33	0.67
Motreff[36]	52	CAD	QCA	Both	4.20±0.8	3.37±0.5	3.28±0.5	
Park[35]	102	CAD	QCA	Both	3.46±0.65			
Christiansen[40]	97	CAD	QCA	Both	4.2±0.5			
Erglis[41]	103	CAD	QCA	Both	3.56±0.53			
Dodge[42]	10	Normal	Angio	Both	4.5±0.5	3.7	3.4	0.63
Medrano-Gracia[10]	217	Normal	CT	Both	3.5±0.8	3.2±0.7	3.0±0.7	0.56
	66	Normal	CT	M	4.1±0.8	3.7±0.6	3.6±0.6	
	151	Normal	CT	F	3.3±0.7	3.1±0.6	2.8±0.7	
Ellwein[43]	55	Normal	CT	Both	4.4			0.67
Waller[44]		CAD	PM	Both	4.0	3.6	3.0	0.60

*Assuming circular in cross-section. Angio: angiography; CAD: coronary artery disease; CT: computed tomography; IVUS: intravascular ultrasound; L main: left main coronary artery; LAD: left anterior descending; LCx: left circumflex coronary artery; PM: post-mortem; QCA: quantitative coronary angiography

Table 2. Diameters of coronary arteries at different bifurcation sites from an atlas of 300 patients without coronary artery disease obtained using CT angiography[10].

LAD/diagonal bifurcation diameters (mm)				Circumflex/obtuse marginal bifurcation diameters (mm)				Right coronary crux diameters (mm)			
LAD (proximal vessel)	LAD (main branch)	Diagonal (side branch)	Finet ratio	Cx (proximal vessel)	Cx (main branch)	OM (side branch)	Finet ratio	RCA (proximal vessel)	Posterior descending (main branch)	Postero-lateral (side branch)	Finet ratio
3.3±0.8	2.7±0.6	2.2±0.6	0.67	3.2±0.7	2.6±0.7	2.4±0.6	0.64	3.4±0.6	2.3±0.6	2.2±0.7	0.75

The numerical values for angles A, B, C and the inflow angle for four different bifurcations (left main, left anterior descending/diagonal, circumflex/obtuse marginal branch, and the crux) are shown in **Table 3**. The inflow angle is the smallest. Angle B is less than angle A or angle C. Angle B for the left main coronary artery is larger than that for the left anterior descending/diagonal or the left circumflex/obtuse marginal branch bifurcations.

While the angles A, B and C add up to 360º in a 2D plane, this is not necessarily true in 3D[10]. The inflow angle is greater in women than men probably because their hearts are smaller and more spherical, causing the coronary arteries to curve towards the apex[10].

Measurements of the bifurcation angle B for the left main coronary artery, undertaken using different technologies and in different patient subgroups, are shown in **Table 3**.

The B angle in degrees for four different bifurcations is shown in **Table 4**. The nomenclature B' is sometimes used to describe the angle between a straight projection of the main vessel centre line and the side branch, as shown in **Figure 3**[10,17-19]. Angle B' is always less than angle B.

Table 3. Bifurcation angles A, B, C and inflow angle for four different coronary artery bifurcations from an atlas derived from 300 normal CT coronary angiograms[10].

	Left main N=217	LAD/diag N=235	LCx/OM N=166	RCA/PD/PL N=171
Angle A, mean±SD	127±21º	144±14º	146±19º	143±16º
Angle B, mean±SD	75±23º	52±17º	55±24º	60±22º
Angle C, mean±SD	139±16º	150±14º	143±15º	142±17º
Inflow angle, mean±SD	8±25º	9±15º	8±18º	3±16º

diag: diagonal; LAD: left anterior descending; LCx: left circumflex artery; OM: obtuse marginal branch; PD: posterior descending branch; PL: posterolateral branch; RCA: right coronary artery

CURVATURE

Blood vessels are seldom straight conduits, with curves and tortuosity being common. Because the heart can be considered to approximate a sphere, the coronary arteries must curve to follow the surface of that sphere[10]. In addition, arteries elongate and become tortuous with age[20]. Atheromatous plaque develops at bifurcations and curves where complex flow occurs[21]. In addition, the curvature of coronary arteries changes during the cardiac

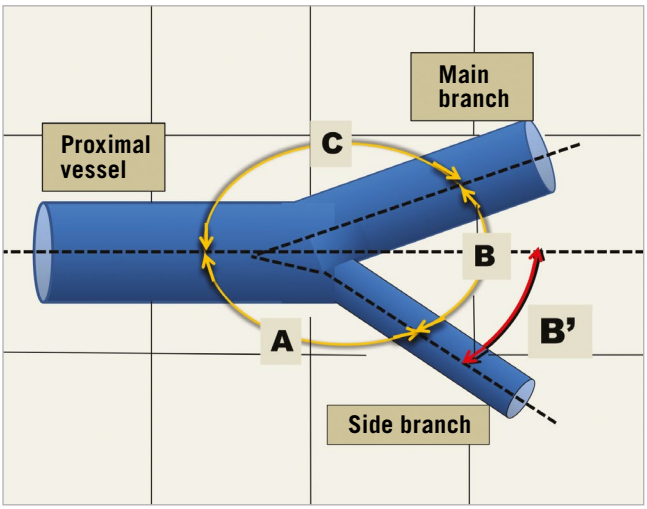

Figure 3. *Derivation of the sometimes used nomenclature, angle B'.*

Table 4. "B" angle (degrees) for four different bifurcations from five different authors.

	Modality	N	Female	Diseased	L main	LAD/diag	LCx/OM	Crux
Pflederer[45]	16-CT	100	NR	Y	B=80±27	B=46±19	B=48±24	B=53±27
Kawasaki[17]	64-CT	209	34%	Y	B'=72±22			B'=61±21
Girasis[16]	3D QCA	266	26%	Y	B=96±24			
Godino[15]	Angio	<75	NR	Y	B=78±28	B=58±19	B=64±21	B=54±19
Rubinshtein[46]	3D QCA	203	31%	Y	B=74±25			

Angio: angiography; Crux: bifurcation of the right coronary artery into posterior descending and posterolateral branches; CT: computed tomography; L main: left main coronary artery; LAD/diag: left anterior descending/first diagonal bifurcation; LCx/OM: left circumflex artery/first obtuse marginal bifurcation; NR: not recorded; QCA: quantitative coronary angiography

cycle, being greatest in systole. Stents cause straightening of the natural curvature of coronary arteries and can influence regional blood flow and alter distributions of indices of wall shear stress. Hence, specific areas, especially at the inlet and outlet of the stent, become more susceptible to neointimal hyperplasia. A limitation of most computational studies examining blood flow patterns through stented vessels to date is the use of linear, static, cylindrical geometric models[22]. Statistical shape analysis is addressed in the **Supplementary Appendix** and **Supplementary Figure 1**.

LEFT MAIN CORONARY ARTERY LENGTH

An atlas derived from 300 normal CT coronary angiograms found the length of the left main coronary artery from ostium to bifurcation to be 10.8±5.1 mm[10]. This generally agrees with the length of the left main coronary artery from other studies, as shown in **Table 5**.

Table 5. Length of the left main coronary artery from different studies.

Author (reference)	Number	Method	Normal/ diseased	Length, mm
Abedin[47]	54	Post-mortem		9.7±4.3
Waller[44]		Post-mortem		1-25
Fox[48]	100	Post-mortem		9.5
	100	Angiography		5.5
Saltissi[49]	54	Angiography	Normal	12.9
	95	Angiograph	Diseased	10.6
Medrano-Gracia[10]	300	Computed tomography	Normal	10.8±5.1

PRACTICAL ANATOMY FOR CORONARY BIFURCATION MODEL CONSTRUCTION

While we have presented detailed bifurcation angle data, it may be practical to construct phantoms with B angles of 30, 60 and 90º and a C angle of, for instance, 140º. The diameters for different bifurcation sites could be chosen from our summarised data **(Table 1)** and could obey fractal geometry guidelines. Models could be constructed with an inflow angle to represent anatomy accurately.

THE CARINA

There are challenges in the manufacturing of bifurcation models with an anatomically correct carina. Attempts usually result in a carina that is too thick and rigid. An anatomically correct carina would aid insights into the efficacy of post-dilatation techniques in bifurcations.

CORONARY STENOSES AND BIFURCATION MODELS

Models can be constructed with stenoses although there are limited published data on this[23]. To validate quantitative angiography, rigid mock vessels with stenoses have been precision drilled in Perspex[1,24]. It is likely that models with stenoses will become more widely used so that devices and strategies can be tested in more realistic situations. In addition, individual patient-specific models can be 3D printed to test strategies before clinical treatment.

NORMAL CORONARY ARTERY ELASTIC RESPONSE

Knowledge of the elastic response of normal and diseased human coronary arteries is important to facilitate construction of realistic bench testing models. The elastic response of a coronary vessel can be expressed in terms of compliance, distensibility, stiffness or elastic modulus, as defined in the **Supplementary Table 1**.

MODELS AND MODEL CONSTRUCTION MATERIALS

In addition to appropriate design, elastic properties and construction material, the model should permit imaging of deployed stents. Historically, the different phantom materials and designs that have been used have limitations.

Troughs in Perspex plates lack anatomical bifurcation accuracy **(Figure 4)**, lack an elastic response and are non-tubular[5]. These phantoms are good for light photography because there is no material between the stent and the camera.

Glass tubes have been used for bifurcation models but have limitations including difficulty manufacturing with anatomical accuracy, high wall rigidity and distortion of light images.

Tubing from aliphatic polyether-based thermoplastic polyurethanes (Tecoflex) has been used when measuring radial strength and assessing longitudinal distortion[25]. This tubing is difficult to make into anatomically correct bifurcations. Photography is difficult because of limited translucency, but the tubing is suitable for micro computed tomography (microCT) imaging.

Casts made from silicone can be anatomically accurate but need to be modified to allow quality light photography **(Figure 4)**. They can be tubular and can have a suitable elasticity. They are suitable for microCT imaging.

With 3D printing, realistic models with normal or diseased anatomy and made from a material with an appropriate elastic response can be constructed.

3D bioprinting and tissue engineering can also be used to fabricate *in vitro* coronary arteries with human-like anatomy, precise wall architecture based on extracellular matrix, multiple cell types including endothelial and smooth muscle cells, and more physiologically and biomechanically relevant microenvironments[26]. These arteries can be tested in bioreactor perfusion systems.

Accurate dimensional and angle data are needed for accurate model construction. Another approach to model construction is first to to print a mould which can be used to cast silicone or other material. There is a wide variety of materials that can be used for 3D printing including plastics, metals, ceramics and even paper.

IMAGING OF STENTS OR SCAFFOLDS IN CORONARY BIFURCATION MODELS

The deployment of stents, scaffolds or other devices in models in a water bath and subsequent steps including proximal

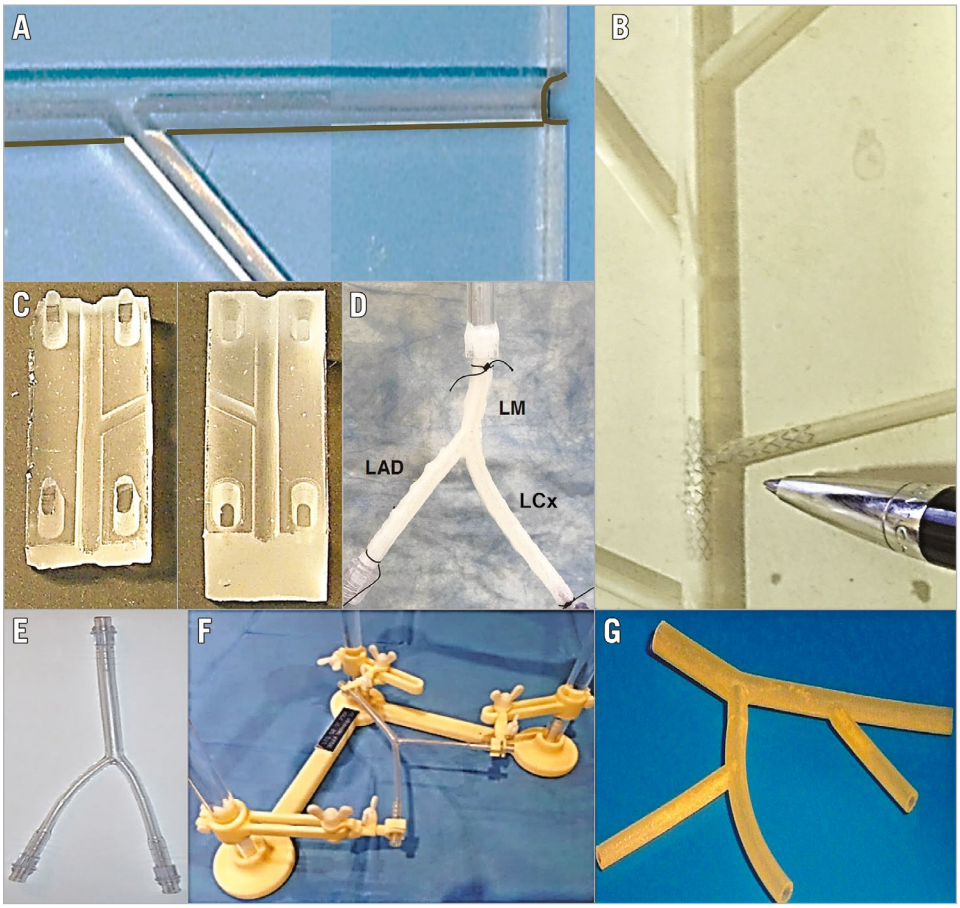

Figure 4. *Some bifurcation models. Our first model (A), constructed in the 1990s, had troughs cut in a poly (methyl methacrylate) acrylic plate (trade names include Perspex)[5]. This was hard and rigid, not tubular and did not obey scaling laws but permitted unrestricted conventional photography. B) A model made from silicone by the Massy group about 20 years ago and used in early experiments with side branch dilatation[50]. C) A model cast from silicone where two halves can be separated to allow conventional photography. The model in panel D is a 3D printed left main coronary artery based on realistic geometry and using polyurethane with hyaluronic acid as sacrifice materials. The bifurcation is mounted on a bioreactor perfusion system. The image in panel E from Finet is constructed from polyvinylchloride (PVC) according to scaling geometry and is fixed in a nylon support to maintain angles between branches (F). The model in panel G was made by 3D printing (also called additive manufacturing) which has the potential for construction of realistic phantoms with normal or diseased anatomy and the potential to be made from a material with an appropriate elastic response.*

optimisation[14], side branch wire access, and additional stenting can be viewed live and recorded fluoroscopically, on video or with serial photography. The device can be removed from the water bath temporarily or permanently so that a particular step can be imaged by, for instance, photography or microCT.

Photography through a microscope is very useful to record images of devices during a wide range of manoeuvres. Multiple images can be acquired easily and in a cost-effective way. Stent deployments have been imaged through a borescope (paediatric endoscope)[27], but this technique has been largely superseded by microCT.

While microCT is limited by cost and time requirements, it does allow unparalleled imaging[28,29]. The images can be readily post-processed with computer algorithms allowing slicing and advanced viewing such as "fly-through". A limitation is that image reconstruction often uses gaming software that distorts the images and precludes accurate length measurement. There may also be problems with contrast resolution between the bench model polymer and the stent or scaffold being tested.

Intravascular ultrasound and optical coherence tomography are useful imaging tools for stents and scaffolds, providing high resolution, and reconstructions to produce 3D patient-specific images[30].

The very high resolution of scanning electron microscopy is useful for examining polymer coatings on stents **(Figure 5)**.

UNIVERSAL TESTING MACHINES

When testing stents on the bench, it may be necessary to apply a measured force (often very small) and measure the distance compressed or elongated (which is usually very small) or conversely

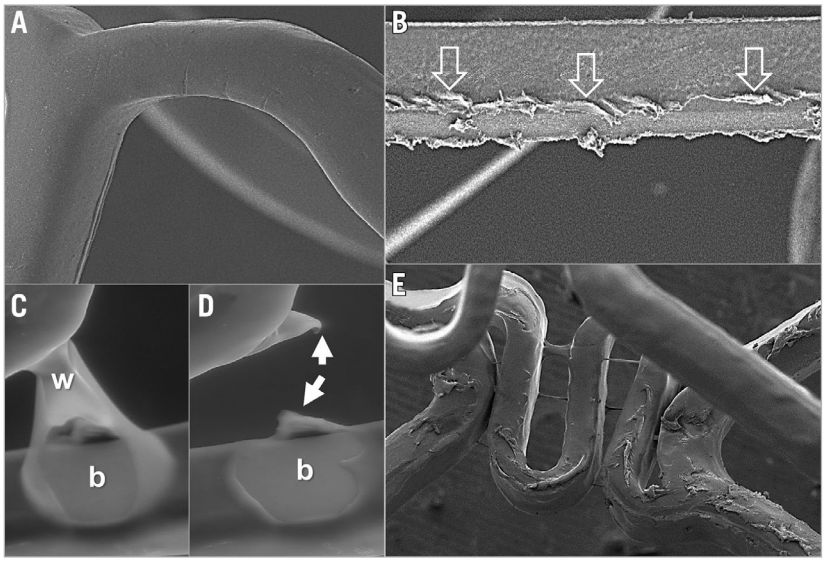

Figure 5. *Polymer coating appearances on scanning electron microscopy. A) The smooth appearance of an undamaged drug-eluting stent polymer coating. The linear polymer coating damage (open arrows) in panel B was caused by withdrawal of an 0.014" percutaneous intervention wire that had been intentionally trapped between the expanded scaffold and model arterial wall. C) A first-generation drug-eluting stent with a polymer web (w) connecting two struts which in panel D had broken, leaving an area of strut bare of polymer coating (b) and some redundant polymer (white arrows). E) Marked irregularity of coating on the luminal surface of a different first-generation drug-eluting stent immediately after deployment.*

elongate or compress a stent or balloon tip by a chosen distance and measure the force required to do this. This may be achieved by using a universal testing machine such as an Instron (Norwood, MA, USA). These machines are basic instruments found in engineering and bench testing facilities.

SPECIMENS TESTED

A report of stent or scaffold testing in bifurcation models would usually document or reference the properties of those devices being tested. Nominal diameters are important to record as different diameters from the same manufacturer may have different designs. Stent lengths and the number of specimens tested should be documented. Stent structural data are important for understanding stent performance in bifurcations. Some of these data may be obtained from the manufacturer or deduced from images. Desirable data that might be included are shown in **Table 6**.

Table 6. Desirable data that may be documented when testing a device.

Construction material
Design features of importance include the shape of hoops, whether there are in-phase or out-of-phase hoops, shape of connectors, and whether connectors differ in the body of the stent from ends
Strut thickness and width for both hoops and connectors
Percentage of the vessel covered by stent or scaffold at a given nominal diameter
Polymer coating thickness and whether the polymer coating is circumferential or otherwise
Potential cell diameter/area (potential orifice size between struts for side branch access)
Crossing profile of device on its delivery system
Radiopacity
If other equipment is used such as balloons, their inflated diameter and whether semi- or non-compliant recorded

TESTING APPARATUS AND TESTING PROCEDURE

In a bench testing report, any testing apparatus should be described in detail and images and/or diagrams provided. It is often necessary to custom-make apparatus to answer specific questions[25,31,32]. Any post-dilatation strategy should be described in detail.

BENCH BIFURCATION TESTING ENDPOINTS

An unanswered clinical bifurcation question may lead to testing of devices on the bench. The question should be clinically relevant, and testing endpoints should be determined by the question. For instance, if the question is scaffold post-dilatation safety without strut fracture then the scaffold would need to be observed for fracture after pressure or diameter post-dilatation challenge.

Stent or scaffold performance characteristics that are important but not specific for bifurcations include recoil, radial strength, flexibility, fracture resistance, longitudinal strength and security from dislodgement off the delivery balloon. Testing for these properties is covered by the US FDA recommendations (dsmica@fda.hhs.gov), and the ISO publication, ISO 25539-2.

Many bifurcation bench studies aim to provide insights into bifurcation stenting or scaffolding by evaluating results obtained

for particular platforms or strategies. Endpoints for bench studies in bifurcations might include the following parameters. Whenever possible, quantitative measurements should be reported.

DEVICE DELIVERABILITY

Different tracks or models with different degrees of tortuosity or stenosis can be used to compare the performance of different devices (ASTM F2394-07). Observation of bench delivery has identified wire bias and wire wrap as causes of delivery problems for dedicated bifurcation stents that deliver over two wires[4]. Bench testing showed that a steerable shaft on a dedicated bifurcation stent permitted device rotation facilitating wire unwrapping and the overcoming of wire bias[33].

DEPLOYMENT QUALITY

Presence or absence of stent or scaffold underexpansion, distortion, cross-sectional area, diameters, eccentricity, and malapposition can be assessed[34,35]. The percentage of the side branch ostium occupied by struts can be assessed.

STENT OR SCAFFOLD DAMAGE

Strut fracture or polymer coating damage can be determined[25,36]. Strut fractures can be counted under direct observation, microscopic observation or by microCT. Polymer coating damage **(Figure 5)** can be imaged with scanning electron microscopy. Ideally there should be quantification of damage[37].

CORRECTION OF DISTORTION

Effectiveness of strategies such as kissing balloon post-dilatation for distortion correction can be assessed[2].

SIDE BRANCH ACCESS

Performance and integrity of different stents or scaffolds or balloons when crossing through the side of devices into the side branch can be evaluated. Cross-sectional stent area and lumen diameter at selected reference landmark locations in the proximal and distal main vessel, bifurcation, and side branch segments can be measured[38].

Percentage of ostial area stenosis can be calculated as follows: (reference segment side branch lumen area minus largest opened stent cell area)/reference side branch lumen area[29].

Limitations of bench testing

Bench testing involves simplification of bifurcation anatomy, bifurcation lesions, or treatment techniques. Bench testing may not predict what occurs in patients. Coronary models do not currently reflect the complexity of human diseased arteries. Models are usually stationary and do not reflect the complex motion of bifurcations during the cardiac cycle[39]. Advanced tissue engineering and 3D bioprinting techniques[26] capable of generating arterial systems with realistic anatomy and function are anticipated to advance the field of bench testing for coronary artery bifurcation treatment in the coming years.

Summary and conclusions

We have provided guidance for bench testing of stents or scaffolds in coronary bifurcations. It is intended to be a guide, and not be prescriptive, as this is an evolving field. These recommendations provide general principles that have been developed by clinicians, scientists, and engineers. The focus is on issues specific to intervention for bifurcation disease that are not covered by ASTM or ISO documents.

Impact on daily practice

We provide data on the anatomy of coronary artery bifurcations, and on the elastic response of coronary arteries to optimise model construction. We also give guidelines for standardised bench assessment of coronary stents, and of percutaneous coronary interventional techniques, including stent deployment, for treating coronary bifurcation lesions. Bench testing may aid clinical practice by elucidating the local haemodynamic forces in bifurcations, by validating quantitative coronary angiography systems, and by facilitating the teaching of interventional techniques. There is potential for 3D printing of bifurcation anatomy specific to a patient, so that different treatment strategies can be assessed, and treatment individualised for that patient.

Conflict of interest statement

T. Mickley is an employee of Boston Scientific Corporation. H. Hojeibane is an employee of Stentys. J. Wooton is an employee of Medtronic Corporation. A. Netravali is an employee of Abbott Vascular. The other authors have no conflicts of interest to declare.

References

1. Grundeken MJ, Ishibashi Y, Ramcharitar S, Tuinenburg JC, Reiber JH, Tu S, Aben JP, Girasis C, Wykrzykowska JJ, Onuma Y, Serruys PW. The need for dedicated bifurcation quantitative coronary angiography (QCA) software algorithms to evaluate bifurcation lesions. *EuroIntervention.* 2015;11:V44-9.

2. Brindise MC, Chiastra C, Burzotta F, Migliavacca F, Vlachos PP. Hemodynamics of Stent Implantation Procedures in Coronary Bifurcations: An in Vitro Study. *Ann Biomed Eng.* 2017;45:542-53.

3. Beier S, Ormiston J, Webster M, Cater J, Norris S, Medrano-Gracia P, Young A, Cowan B. Dynamically scaled phantom phase contrast MRI compared to true-scale computational modeling of coronary artery flow. *J Magn Reson Imaging.* 2016;44:983-92.

4. Ormiston JA, Webster M, Webber B. Percutaneous Coronary Intervention for Bifurcation Lesions: Bench Testing and the Real World, in Waksman R and Ormiston JA, eds. Bifurcation Stenting. Chichester, UK: Wiley-Blackwell; 2012. p.83-88.

5. Ormiston JA, Webster MW, Ruygrok PN, Stewart JT, White HD, Scott DS. Stent deformation following simulated side-branch dilatation: a comparison of five stent designs. *Catheter Cardiovasc Interv.* 1999;47:258-64.

6. Murray C. The Physiology Principle of Minimum Work. I. The Vascular System and Cost of Blood Volume. *Proc Natl Acad Sci U S A.* 1926;12:207-14.

7. Huo Y, Kassab G. A scaling law of vascular volume. *Biophys J.* 2009;96:347-53.

8. Finet G, Gilard M, Perrenot B, Rioufol G, Montreff P, Gavit L, Prost R. Fractal geometry of arterial coronary bifurcations: a quantitative coronary angiography and intravascular ultrasound analysis. *EuroIntervention.* 2007;3:490-8.

9. Finet G, Huo Y, Rioufol G, Ohayon J, Guerin P, Kassab GS. Structure-function relation in the coronary artery tree: from fluid dynamics to arterial bifurcations. *EuroIntervention.* 2010;6 Suppl J:J10-5.

10. Medrano-Gracia P, Ormiston J, Webster M, Beier S, Young A, Ellis C, Wang C, Smedby Ö, Cowan B. A computational atlas of normal coronary artery anatomy. *EuroIntervention.* 2016;12:845-54.

11. Abizaid AS, Mintz GS, Abizaid A, Mehran R, Lansky AJ, Pichard AD, Satler LF, Wu H, Kent KM, Leon MB. One-year follow-up after intravascular ultrasound assessment of moderate left main coronary artery disease in patients with ambiguous angiograms. *J Am Coll Cardiol.* 1999;34:707-15.

12. Javier SP, Mintz GS, Popma JJ, Pichard AD, Kent KM, Satler LF, Leon MB. Intravascular ultrasound assessment of the magnitude and mechanism of coronary artery lumen tapering. *Am Heart J.* 1995;75:177-80.

13. Louvard Y, Thomas M, Dzavik V, Hildick-Smith D, Galassi AR, Pan M, Burzotta F, Zelizko M, Dudek D, Ludman P, Sheiban I, Lassen JF, Darremont O, Kastrati A, Ludwig J, Iakovou I, Brunel P, Lansky A, Meerkin D, Legrand V, Medina A, Lefèvre T. Classification of coronary artery bifurcation lesions and treatments: time for a consensus! *Catheter Cardiovasc Interv.* 2008;71:175-83.

14. Lassen JF, Holm NR, Stankovic G, Lefèvre T, Chieffo A, Hildick-Smith D, Pan M, Darremont O, Albiero R, Ferenc M, Louvard Y. Percutaneous coronary intervention for coronary bifurcation disease: consensus from the first 10 years of the European Bifurcation Club meetings. *EuroIntervention.* 2014;10:545-60.

15. Godino C, Al-Lamee R, La Rosa C, Morici N, Latib A, Ielasi A, Di Mario C, Sangirogi GM, Colombo A. Coronary left main and non-left main bifurcation angles: how are the angles modified by different bifurcation stenting techniques? *J Interv Cardiol.* 2010;23:382-93.

16. Girasis C, Serruys PW, Onuma Y, Colombo A, Holmes DR Jr, Feldman TE, Bass EJ, Leadley K, Dawkins KD, Morice MC. 3-Dimensional bifurcation angle analysis in patients with left main disease: a substudy of the SYNTAX trial (SYNergy Between Percutaneous Coronary Intervention with TAXus and Cardiac Surgery). *JACC Cardiovasc Interv.* 2010;3:41-8.

17. Kawasaki T, Koga H, Senikawa T, Orita Y, Mito T, Gotou Y, Shintani Y, Tanaka A, Tanaka H. The bifurcation study using 64 multislice computed tomography. *Catheter Cardiovasc Interv.* 2009;73:653-8.

18. Dzavik V, Colombo A. The absorb bioresorbable scaffold in coronary bifurcations: insights from bench testing. *JACC Cardiovasc Interv.* 2014;7:81-8.

19. Dzavik V, Kharbanda R, Ivanov J, Ing DJ, Bui S, Mackie K, Ramsamujh R, Barolet A, Schwartz L, Seidelin PH. Predictors of long-term outcome after crush stenting of coronary bifurcation lesions: importance of bifurcation angle. *Am Heart J.* 2006;152:762-9.

20. Hutchings GM, Bulkley BH, Miner MM, Boitnott JK. Correlation of age and heart weight with tortuosity and caliber of normal human coronary arteries. *Am Heart J.* 1977;94:196-202.

21. Prosi M, Perktold K, Ding Z, Friedman MH. Influence of curvature on pulsatile coronary artery flow in a realistic bifurcation model. *J Biomech.* 2004;37:1767-75.

22. LaDisa JF Jr, Olsen LE, Douglas HA, Warltier DC, Kersten JR, Pagel PS. Alterations in regional vascular geometry produced by theoretical stent implantation influence distributions of wall shear stress: analysis of a curved coronary artery using 3D computational fluid dynamics modeling. *Biomed Eng Online.* 2006;5:40.

23. Hikichi Y, Umezu M, Node K, Iwasaki K. Reduction in incomplete stent apposition area caused by jailed struts after single stenting at left main bifurcation lesions: micro-CT analysis using a three-dimensional elastic bifurcated coronary model. *Cardiovasc Interv Ther.* 2017;32:12-7.

24. Girasis C, Schuurbiers JC, Onuma Y, Aben JP, Weijers B, Boersma E, Wentzel J, Serruys PW. Two-dimensional quantitative coronary angiographic models for bifurcation segmental analysis: in vitro validation of CAAS against precision manufactured plexiglass phantoms. *Catheter Cardiovasc Interv.* 2011;77:830-9.

25. Ormiston JA, Webber B, Ubod B, White J, Webster MW. Stent longitudinal strength assessed using point compression: insights from a second-generation, clinically related bench test. *Circ Cardiovasc Interv.* 2014;7:62-9.

26. Duan B. State-of-the-art Review of 3D Bioprinting for Cardiovascular Tissue Engineering. *Ann Biomed Eng.* 2017;45:195-209.

27. Ormiston JA, Currie E, Webster MW, Kay P, Ruygrok PN, Stewart JT, Padgett RC, Panther MJ. Drug-eluting stents for coronary bifurcations: insights into the crush technique. *Catheter Cardiovasc Interv.* 2004;63:332-6.

28. Ormiston JA, Webber B, Webster MW. Stent longitudinal integrity bench insights into a clinical problem. *JACC Cardiovasc Interv.* 2011;4:1310-7.

29. Ormiston JA, Webster MW, Webber B, Stewart JT, Ruygrok PN, Hatrick RI. The "crush" technique for coronary bifurcation stenting: insights from micro-computed tomographic imaging of bench deployments. *JACC Cardiovasc Interv.* 2008;1:351-7.

30. Doulaverakis C, Tsampoulatidis I, Antoniadis A, Chatzizisis Y, Giannopoulos A, Kompatsiaris I, Giannoglou GD. IVUSAngio tool: a publicly available software for fast and accurate 3D reconstruction of coronary arteries. *Comput Biol Med.* 2013;43:1793-803.

31. Ormiston JA, Webber B, Ubod B, White J, Webster MW. Coronary stent durability and fracture: an independent bench comparison of six contemporary designs using a repetitive bend test. *EuroIntervention.* 2015;10:1449-55.

32. Ormiston JA, Dixon SR, Webster MW, Ruygrok PN, Stewart JT, Minchington I, West T. Stent longitudinal flexibility: a comparison of 13 stent designs before and after expansion. *Catheter Cardiovasc Interv.* 2000;50:120-4.

33. Ormiston J, Darremont O, Iwasaki K, Murasato Y, Hikichi Y, Webber B, Webster M. Lessons from the real bench: non-BRS. *EuroIntervention.* 2015;11 Suppl V:V27-30.

34. Finet G, Gilard M, Perrenot B, Rioufol G, Motreff P, Gavit L, Prost R. Fractal geometry of arterial coronary bifurcations: a quantitative coronary angiography and intravascular ultrasound analysis. *EuroIntervention.* 2008;3:490-8.

35. Park DW, Hong MK, Mintz GS, Lee CW, Song JM, Han KH, Kang DH, Cheong SS, Song JK, Kim JJ, Weissman NJ, Park SW, Park SJ. Two-year follow-up of the quantitative angiographic and volumetric intravascular ultrasound analysis after nonpolymeric paclitaxel-eluting stent implantation: late "catch-up" phenomenon from the ASPECT study. *J Am Coll Cardiol.* 2006;48:2432-9.

36. Motreff P, Rioufol G, Gilard M, Caussin C, Ouchchane L, Souteyrand G, Finet G. Diffuse atherosclerotic left main coronary artery disease unmasked by fractal geometric law applied to quantitative coronary angiography: an angiographic and intravascular ultrasound study. *EuroIntervention.* 2010;5:709-15.

37. Levy Y, Mandler D, Weinberger J, Domb AJ. Evaluation of drug-eluting stents' coating durability--clinical and regulatory implications. *J Biomed Mater Res B Appl Biomater.* 2009;91:441-51.

38. Foin N, Torii R, Mortier P, De Beule M, Viceconte N, Chan PH, Davies JE, Xu XY, Krams R, Di Mario C. Kissing balloon or sequential dilatation of the side branch and main vessel for provisional stenting of bifurcations: lessons from micro-computed tomography and computational simulations. *JACC Cardiovasc Interv.* 2012;5:47-56.

39. Kim YH, Lee JH, Roh JH, Ahn JM, Yoon SH, Park DW, Lee JY, Yun SC, Kang SJ, Lee SW, Lee CW, Seung KB, Shin WY, Lee NH, Lee BK, Lee SG, Nam CW, Yoon J, Yang JY, Hyon MS, Lee K, Jang JS, Kim HS, Park SW, Park SJ. Randomized Comparisons Between Different Stenting Approaches for Bifurcation Coronary Lesions With or Without Side Branch Stenosis. *JACC Cardiovasc Interv.* 2015;8:550-60.

40. Christiansen EH, Lassen JF, Anderson HR, Krusell LR, Kristensen SD, Botker HE, Thuesen L. Outcome of unprotected left main percutaneous coronary intervention in surgical low-risk, surgical high-risk, and acute myocardial infarction patients. *EuroIntervention.* 2006;1:403-8.

41. Erglis A, Narbute I, Jegere S, Mintale I, Zakke I, Strazdins U, Saltups A. A randomized comparison of paclitaxel-eluting stents versus bare-metal stents for treatment of unprotected left main coronary artery stenosis. *J Am Coll Cardiol.* 2007;50:491-7.

42. Dodge JT Jr, Brown BG, Bolson EL, Dodge HT. Lumen diameter of normal human coronary arteries. Influence of age, sex, anatomic variation and left ventricular hypertrophy. *Circulation.* 1992;86:232-46.

43. Ellwein L, Marks DS, Migrino RQ, Foley WD, Sherman S, LaDisa JF Jr. Image-based quantification of 3D morphology for bifurcations in left coronary artery: Application to stent design. *Catheter Cardiovasc Interv.* 2016;87:1244-55.

44. Waller BF, Orr CM, Slack JD, Pinkerton CA, Van Tassel J, Peters T. Anatomy, histology, and pathology of coronary arteries: a review relevant to new interventional and imaging techniques--Part I. *Clin Cardiol.* 1992;15:451-7.

45. Pflederer T, Ludwig J, Ropers D, Daniel WG, Achenbach S. Measurement of coronary artery bifurcation angles by multidetector computed tomography. *Invest Radiol.* 2006;41:793-8.

46. Rubinshtein R, Lerman A, Spoon D, Rihal C. Anatomic features of the left main coronary artery and factors associated with its bifurcation angle: a 3-dimensional quantitative coronary angiographic study. *Catheter Cardiovasc Interv.* 2009;80:304-9.

47. Abedin Z, Goldberg J. Origin and length of left main coronary artery: its relationship to height, weight, sex, age, pattern of coronary distribution, and presence or absence of coronary artery disease. *Cathet Cardiovasc Diagn.* 1978;4:335-40.

48. Fox C, Davies MJ, Webb-Peploe MM. Length of left main coronary artery. *Br Heart J.* 1973;35:796-8.

49. Saltissi S, Webb-Peploe MM, Coltart D. Effect of variation in coronary artery anatomy on distribution of stenotic lesions. *Br Heart J.* 1979;42:186-91.

50. Lefèvre T, Louvard Y, Morice MC, Loubeyre C, Piéchaud JF, Dumas P. Stenting of bifurcation lesions: a rational approach. *J Interv Cardiol.* 2001;14:573-85.

51. Gregg DE, Green HD, Wiggers CJ. Phasic variations in peripheral coronary resistance and their determinants. *Am J Physiol.* 1935;112:362-73.

52. Patel DJ, Janicki JS. Static elastic properties of the left coronary circumflex artery and the common carotid artery in dogs. *Circ Res.* 1970;2:149-58.

53. Kassab GS, Molloi S. Cross-sectional area and volume compliance of porcine left coronary arteries. *Am J Physiol Heart Circ Physiol.* 2001;281:H623-8.

54. Gow BS, Hadfield CD. The elasticity of canine and human coronary arteries with reference to postmortem changes. *Circ Res.* 1979;45:588-94.

55. Tomoike H, Ootsubo H, Sakai K, Kikuchi Y, Nakamura M. Continuous measurement of coronary artery diameter in situ. *Am J Physiol.* 1981;240:H73-9.

56. Holzapfel GA, Mulvihill JJ, Cunnane EM, Walsh MT. A computational approach for analyzing the mechanics of atherosclerotic plaques: a review. *J Biomech.* 2014;47:859-69.

57. Medrano-Gracia P, Ormiston J, Webster M, Beier S, Ellis C, Wang C, Smedby Ö, Young A, Cowan B. A Study of Coronary Bifurcation Shape in a Normal Population. *J Cardiovasc Transl Res.* 2017;10:82-90.

Supplementary data

Supplementary Appendix. Averaging coronary artery bifurcation shape (statistical shape analysis).

Supplementary Figure 1. Modes of variation.

Supplementary Table 1. Summary of published data on arterial volume compliance, distensibility, and Young's modulus for canine and porcine models and in humans.

The supplementary data are published online at: http://www.pcronline.com/eurointervention/130th_issue/292

Supplementary data

Supplementary Appendix. Averaging coronary artery bifurcation shape (statistical shape analysis).

The rapid evolution of 3D printing means that it is no more difficult to create a bifurcation with non-circular cross-section, with local wall irregularities, tortuosity, and out of plane daughter vessels than it is to create the confluence of three straight circular pipes.

If we consider hypothetically 100 left main bifurcations stored in computer memory as several thousand 3D points on the luminal surface (known as a “point cloud”), the complexity of local irregularities, tortuosity, non-circular cross-section, and curvature are all captured. When testing a stent in this sample, the question of how to determine the average luminal surface shape (and perhaps one or two standard deviations each side of the mean) arises[57].

The simplest approach is to choose a small number of parameters such as vessel diameter and bifurcation angle, and to find their respective averages. By making additional assumptions, such as circular cross section, and that all vessels are co-planar and straight, a bench model can be created. While useful, there are limitations with this approach because much of the complexity and richness of the original data is lost. In addition, the assumptions are not likely to be exactly correct. Furthermore, there may be a complex relationship between the averaged parameters, for example bifurcation angle is correlated with vessel diameter. At the opposite end of the spectrum, an alternative approach is to create 100 separate models retaining each patient’s full anatomical detail, and to deploy a stent in each of them.

Between these two extremes is the field of “statistical shape analysis”. This enables the calculation of true shape averages and has been used to average the complex 3D shape of, the coronary arteries[57]. Within the field of computational biology, shape analysis allows the generation of true average shapes unencumbered by the need to make assumptions, or to simplify the problem. The specific techniques commonly used include Procrustes analysis, principal component analysis (PCA), landmark identification, non-rigid registration, and atlasing.

The ability to create true 3D shape averages (±1-2 standard deviations) and to 3D print these, captures a much higher degree of shape complexity, and represents a significant opportunity for the advancement of bench testing (**Supplementary Figure 1**).

Another advantage of 3D printing is the use of scaling, where 3D prints of coronaries can be enlarged. This has many advantages, including demonstration purposes, teaching, and imaging, and is particularly useful for evaluating small diameter coronary arteries. This may enable the innovative use of imaging tools such as 4D magnetic resonance imaging which currently has insufficient resolution for direct imaging.

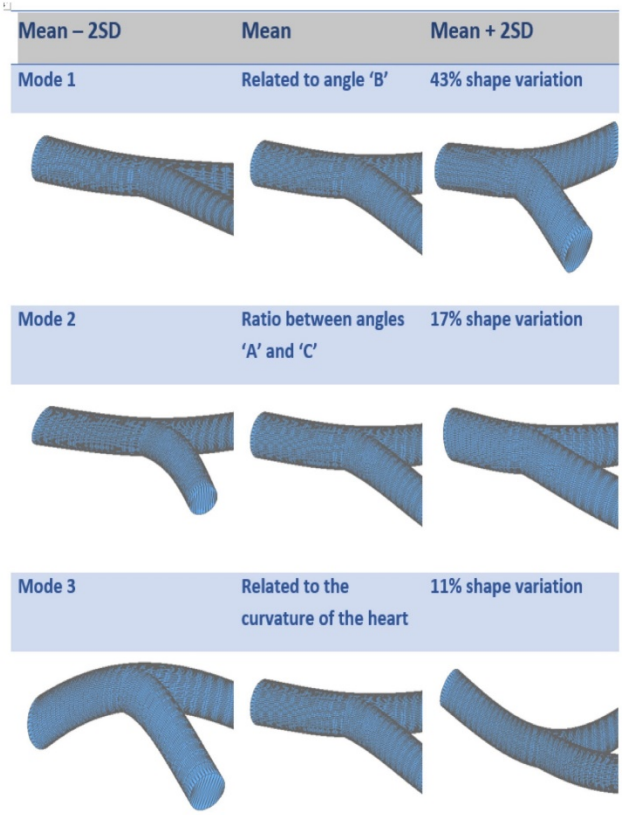

Supplementary Figure 1. Modes of variation.

Shown are modes of variation from a statistical model of shape built from a CT atlas of 446 bifurcations including the left main, left anterior descending/first diagonal, circumflex/first obtuse marginal and right coronary crux bifurcations. The field of "statistical shape analysis" enables the calculation of true shape averages and has been used to average the complex 3D shape of the coronary arteries. Within the field of computational biology, shape analysis allows the generation of true average shapes unencumbered by the need to make assumptions, or to simplify the problem. The specific techniques commonly used include Procrustes analysis, principal component analysis (PCA), landmark identification, non-rigid registration, and atlasing.

.

Supplementary Table 1. Summary of published data on arterial volume compliance, distensibility, and Young's modulus for canine and porcine models and in humans.

	Arterial volume compliance, ml/mmHg		**Diameter, mm**	**Pressure, mmHg**
Gregg[51]	≈1x10^{-3}	canine		Mean 80
Patel[52]	5x10^{-4}	canine		
Kassab[53]	(1.1±0.45) x 10^{-3}	canine		
	Distensibility, mmHg^{-1} x 10^{-3}			
Gow[54]	2.2±0.5	human	4.9	70-110
Patel	2.6-3.6	canine	2.6-3.6	60-140
Tomoike[55]	0.8-2.6	porcine	0.8-2.6	60-140
Kassab	0.68-1.6	porcine	2.6	60-140
	Young's modulus, Kpa			
Holzapfel[56]	700-1,500	human		